FISEVIER

Contents lists available at ScienceDirect

Journal of Magnetism and Magnetic Materials

journal homepage: www.elsevier.com/locate/jmmm





Transition metal-doped chalcogenide perovskite magnetic semiconductor BaZrS₃

Zhonghai Yu^{a,1}, Chenhua Deng^{b,1}, Sen Kong^a, Haolei Hui^c, Jiale Guo^a, Qizhong Zhao^a, Fanghua Tian^a, Chao Zhou^a, Yin Zhang^a, Sen Yang^{a,*}, Hao Zeng^{c,*}

- ^a School of Physics, Xi'an Jiaotong University, Xi'an, Shaanxi 710049, PR China
- ^b Department of Chemistry, Taiyuan Normal University, JinZhong, Shanxi 030619, PR China
- ^c Department of Physics, University at Buffalo, The State University of New York, Buffalo, NY 14260, United States

ARTICLE INFO

Keywords: Diluted magnetic semiconductors Chalcogenide perovskite Room temperature ferromagnetism Exchange interactions

ABSTRACT

Diluted magnetic semiconductors (DMSs) are an important type of materials for spintronic applications. Conventional DMSs are typically based on transition metal doped III-V and II-VI materials such as GaAs and CdSe. In this work, we show that a new DMS material can be realized by transition metal doping in BaZrS₃, a prototypical chalcogenide perovskite semiconductor. Mn and Fe elements are doped into the BaZrS₃ lattice with a concentration of up to 5%. In particular, Fe-doped BaZrS₃ exhibits room temperature ferromagnetism.

1. Introduction

Spintronics exploits the spin degree of freedom of electrons to realize information storage and logic function[1–3]. Spintronic devices offer advantages such as faster speed, ultra-low heat dissipation, and nonvolatility, making them attractive for future electronics. DMSs[3-8] are one type of spintronic materials, where long range magnetism typically originates from carrier-dopant exchange interactions. Compared with ordinary magnetic materials, magnetism and carrier spin polarization in DMSs can be readily tuned by electric gating or light irradiation[9]. However, DMSs typically have relatively low Curie temperature (T_C), which limit their practical applications. Room temperature magnetism has been found in doped and undoped oxide semiconductors[10-14]. However, the origin of magnetism is controversial, and gate and light tunable magnetism and carrier spin polarization in such systems remain elusive. Finding true room temperature magnetic semiconductor is a key challenge in the field of semiconductor spintronics[15-18].

The difficulty in realizing room temperature DMSs in either II-VI and III-V semiconductors, and controversy in unambiguous demonstration of carrier spin polarization in oxide DMSs have established the need for investigating new semiconducting host materials for DMSs. Recently, chalcogenide perovskites have received increased attention as an emerging ionic semiconductor family with fascinating optoelectronic

properties[19–24]. The chalcogenide perovskites have a general formula of ABX3, where A represents a group II cation (e.g., Ca^{2+} , Sr^{2+} or Ba^{2+}), B represents a group IV transition metal (e.g., Ti^{4+} , Zr^{4+} or Hf^{4+}) and X is a chalcogen anion (S^2 or Se^2). By replacing O with S or Se, the bandgap of chalcogenide perovskite is reduced to the visible-IR range. With extraordinarily high absorption coefficients near the visible band gap energy[22,25], and high stability against oxidation, moisture, and pressure[20,26], chalcogenide perovskites are attractive for photovoltaics and optoelectronics applications[21,27,28]. Recent work has shown that chalcogenide perovskite BaZrS3 can be substitutionally doped with Ti with a small concentration to effectively low the band gap [29,30]. It is therefore reasonable to postulate that Zr can be substituted by magnetic transition metal elements such as Mn and Fe to modify its magnetic properties.

In this work, we report the synthesis and characterization of Mn and Fe doped $BaZrS_3$, with the goal of achieving a new type of DMS. We found that Zr can be substituted by Mn and Fe by a small percentage up to 5%, beyond which impurity phase starts to emerge. The doped $BaZrS_3$ show ferromagnetic properties, with their magnetization increasing with increasing doping concentration. In particular, Fe-doped $BaZrS_3$ exhibits room temperature ferromagnetism, with a relatively large coercivity.

E-mail addresses: yang.sen@xjtu.edu.cn (S. Yang), haozeng@buffalo.edu (H. Zeng).

^{*} Corresponding authors.

 $^{^{1}}$ These authors contribute equally to this work.

2. Materials and methods

BaCO $_3$, ZrO $_2$, MnO $_2$ and Fe $_3$ O $_4$ powder (99.9% purity) were used as starting materials to make Ba(Zr $_{1-x}$ Mn $_x$)O $_3$ powder with x=0.0, 0.01. 0.02, 0.03, 0.05 and Ba(Zr $_{1-x}$ Fe $_x$)O $_3$ powder with x=0.02, 0.05. The molar ratio of Ba: (Zr + Mn) and Ba: (Zr + Fe) was 1: 1. The mixture was ball milled and calcinated at 1100 °C for 4 hr. The Ba(Zr $_{1-x}$ Mn $_x$)O $_3$ and

 ${\rm Ba}({\rm Zr_{1-x}Fe_x}){\rm O_3}$ powder was then sulfurized using ${\rm CS_2}$. ${\rm CS_2}$ was carried by Ar gas at a flow rate of 16–18 ml/min. The gas flow was only turned on/off at 800 °C during temperature ramping up/down. Sodium hydroxide solution was used for reacting with excess ${\rm CS_2}$ from the exhaust.

Powder X-ray diffraction (XRD) spectra were acquired using a Bruker D8 ADVANCE system operating at 1.76 kW (40 kV, 44 mA) with a Cu target. The powder XRD measurements were performed under θ -2 θ

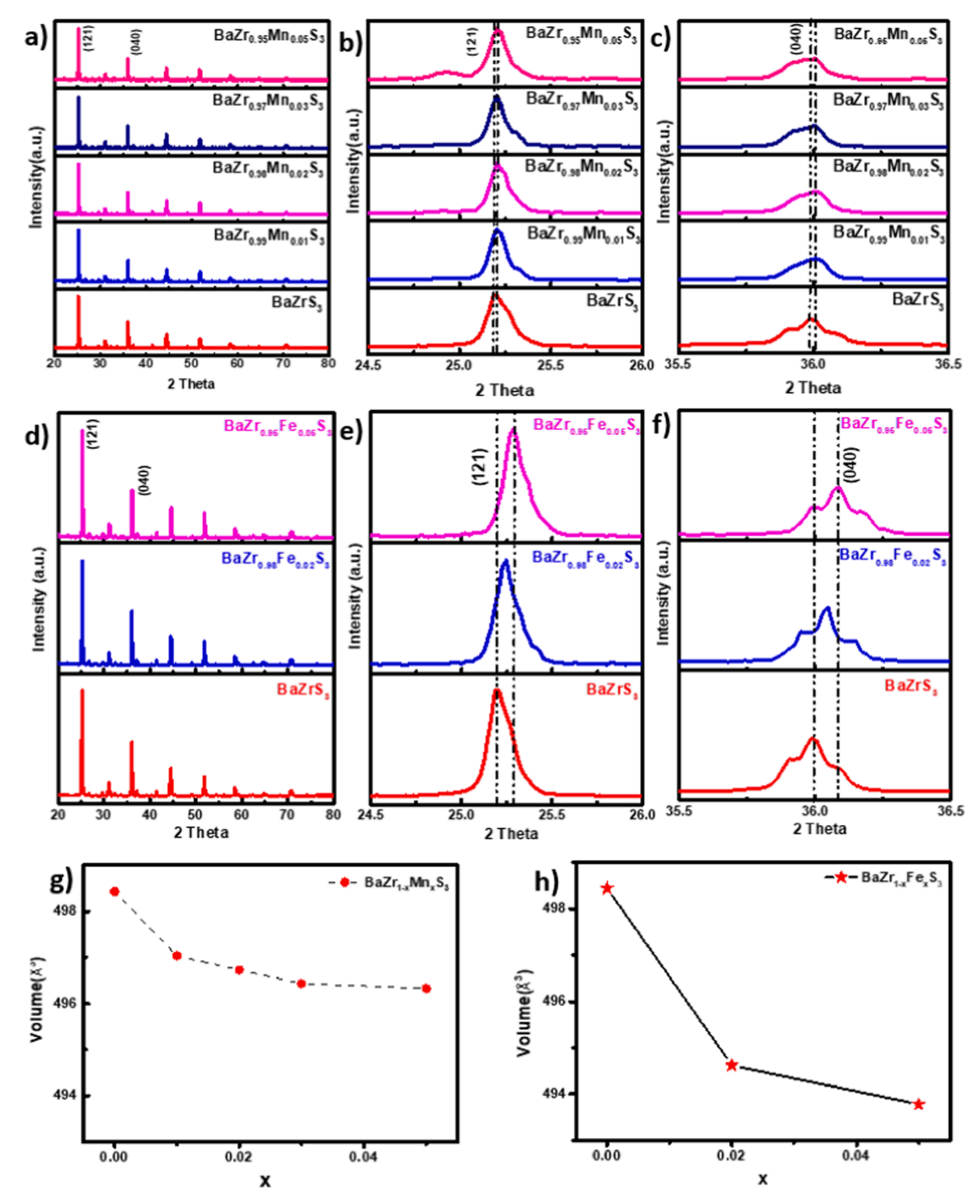


Fig. 1. a) XRD patterns of Ba(Zr_{1-x}Mn_x)S₃ powder samples for x = 0, 0.01, 0.02, 0.03, 0.05; The enlarged view of b) (121) peak, c) (040) peak of Ba(Zr_{1-x}Mn_x)S₃; g) lattice volume of the Ba(Zr_{1-x}Mn_x)S₃; d) XRD patterns of Ba(Zr_{1-x}Fe_x)S₃ powder samples for x = 0, 0.02, 0.05. The enlarged view of e) (121) peak, f) (040) peak of Ba (Zr_{1-x}Fe_x)S₃; h) lattice volume of the Ba(Zr_{1-x}Fe_x)S₃.

scanning mode and continuous scanning with a step size of 0.02°. Raman spectra were obtained from a HORIBA Raman spectrometer working under 532 nm laser excitation. The scanning electron microscopy (SEM) images and energy dispersive X-ray spectroscopy (EDX) analysis were acquired from a Focused Ion Beam-Scanning Electron Microscope (FIB-SEM) – Carl Zeiss AURIGA CrossBeam with an Oxford EDS system. The absorption spectra were collected from a Cary series UV–Vis-NIR spectrophotometer measured from 400 nm to 800 nm. The magnetic (M–H) measurements were performed using a Superconducting Quantum Interface Device (SQUID) magnetometer (Quantum Design, MPMS-XL-5).

3. Results and discussion

XRD spectra of $Ba(Zr_{1-x}Mn_x)S_3$ power samples for x = 0, 0.01, 0.02,0.03, 0.05 and $Ba(Zr_{1-x}Fe_x)S_3$ powder samples for $x=0,\,0.02,\,0.05$ are shown in Fig. 1a and 1d. All peaks match with the standard PDF card JCPDS 00-015-0327 of BaZrS₃ with distorted perovskite structure (Pnma space group). Enlarged views of the strongest peaks (121) and (040) of $Ba(Zr_{1-x}Mn_x)S_3$ are shown in Fig. 1b, c, and of $Ba(Zr_{1-x}Fe_x)S_3$ in Fig. 1e, f; It can be seen that as the doping concentration of manganese and iron increases, the peak positions of (121) and (040) shift to higher angles. The amount of shift is 0.023° and 0.020° for Mn-doped, and 0.082° and 0.1° for Fe-doped samples, respectively, at a doping concentration of x = 0.05. This indicates that the volume of the lattice decreases with increasing doping concentration, as can be seen from Fig. 1g and 1 h. The volume reduction is 0.42% for $Ba(Zr_{0.95}Mn_{0.05})S_3$ and 0.94% for Ba(Zr_{0.95}Fe_{0.05})S₃. The volume reduction suggests that the Mn and Fe elements have been incorporated in the perovskite lattice rather than forming interstitials, as otherwise it would increase the volume. The $Ba(Zr_{1-x}Mn_x)S_3$ and $Ba(Zr_{1-x}Fe_x)S_3$ lattices are stable without phase separation up to x = 0.05, above which impurity peaks start to appear, as can be seen from Figure S1.

The Raman spectra of $\mathrm{Ba}(\mathrm{Zr}_{1-x}\mathrm{Mn_x})\mathrm{S}_3$ and $\mathrm{Ba}(\mathrm{Zr}_{1-x}\mathrm{Fe_x})\mathrm{S}_3$ with different doping concentration measured at room temperature are shown in Fig. 2. Several Raman modes can be identified, including B_{2g}^1 , A_g^6 , B_{2g}^6 and B_{3g}^5 . There is no obvious peak shifts within our doping limit. It is interesting to observe that the intensity of the B_{3g}^5 peak increases with increasing doping concentration from 0 to 0.05. This peak was earlier attributed to the forbidden longitudinal-optical (LO)-phonon scattering of BaZrS_3 observed using 676 nm resonant excitation, corresponding mainly to the Zr -S stretching mode[26]. In this work, the 532 nm off-resonance excitation leads to very weak features in this wavenumber region in pristine BaZrS_3 . However, with Mn and Fe substitution of the Zr-sites, the selection rules can be relaxed due to local structural distortion. Therefore, the increase in intensity of this mode with

increasing doping concentration is an indication that Mn and Fe are substitutionally doped into the Zr-site of the perovskite lattice.

Typical SEM images of $Ba(Zr_{1-x}Mn_x)S_3$ and $Ba(Zr_{1-x}Fe_x)S_3$ powder samples with x=0.05 are shown in Fig. 3 (a) and (b). It can be seen that the samples possess uniform grains with grain sizes of a few microns. Meanwhile, the sample composition was analyzed by EDX (as shown in Fig. 3 (c) and (d)). The composition ratio of Ba/Zr/Fe/S is 24.93: 22.17: 0.94: 51.96 for $Ba(Zr_{1-x}Fe_x)S_3$, and Ba/Zr/Mn/S is 24.47: 21.31: 0.87: 53.36 for $Ba(Zr_{1-x}Mn_x)S_3$. Fe and Mn concentration from EDX analysys is close to 4%, slightly lower than the nominal concentration of x=0.05. There is a deviation from the stoichiometric 1:1:3 ratio with substantial sulfur deficiency due to sulfur vacancy formation from the high processing temperature, which is consistent with our previously work [21,27].

We characterized the bandgap of $Ba(Zr_{1-x}Mn_x)S_3$ and $Ba(Zr_{1-x}Fe_x)S_3$ using ultraviolet–visible (UV–Vis) absorption spectroscopy, and extracted the bandgap using the Tauc plot. The Tauc plots of $Ba(Zr_{1-x}Mn_x)S_3$ and $Ba(Zr_{1-x}Fe_x)S_3$, with different doping percentages are shown in Fig. 4. It can be seen that without doping, the bandgap of $BaZrS_3$ is ~ 1.78 eV. With increasing Mn and Fe doping concentration, the bandgap decreases monotonically. The bandgap drops to 1.58 eV for $Ba(Zr_{0.95}Mn_{0.05})S_3$ as shown in Fig. 4a, and 1.63 eV for $Ba(Zr_{0.95}Fe_{0.05})S_3$ as shown in Fig. 4b. Previous theoretical work has shown that the valence band maximum (VBM) states of chalcogenide perovskites are composed of predominantly chalcogen p orbitals, while the conduction band minimum (CBM) states are composed of predominantly transition metal d orbitals. Compared with Zr 4d orbitals, the Mn and Fe 3d orbitals are significantly deeper in energy. By partially replacing Zr with Mn and Fe, the CBM moves downward and thus narrows the bandgap.

The substitutional doping of Mn and Fe in BaZrS3 at the Zr site is confirmed by Raman, XRD and UV-vis spectroscopies. The incorporation of magnetic transition metal elements such as Mn and Fe in the lattice is expected to substantially change the magnetic properties of BaZrS₃, which is otherwise non-magnetic. To investigate the magnetism of these doped samples, the magnetic hysteresis loops of $Ba(Zr_{1-x}Mn_x)S_3$ and $Ba(Zr_{1-x}Fe_x)S_3$ power samples with x=0.02 and 0.05 were measured at different temperatures, and shown in Fig. 5. It can be seen that the magnetization increases with increasing doping concentration for both Mn- and Fe-doped samples. However, they show contrasting behaviors. For $Ba(Zr_{1-x}Mn_x)S_3$, both doping levels of 0.02 and 0.05 show essentially paramagnetic behavior at room temperature, as seen by the linear field dependence of magnetization. Ferromagnetism is only observed at around 2 K. This is similar to that observed in Mn-doped semiconductor quantum dots such as CdSe and PbS[3,31-33]. In contrast, Ba(Zr_{1-x}Fe_x)S₃ shows clear ferromagnetic behavior at room temperature for both doping concentrations, as can be seen from Fig. 5 (c) and (d). The coercivity is unusually high for a DMS, at 3,760 Oe at

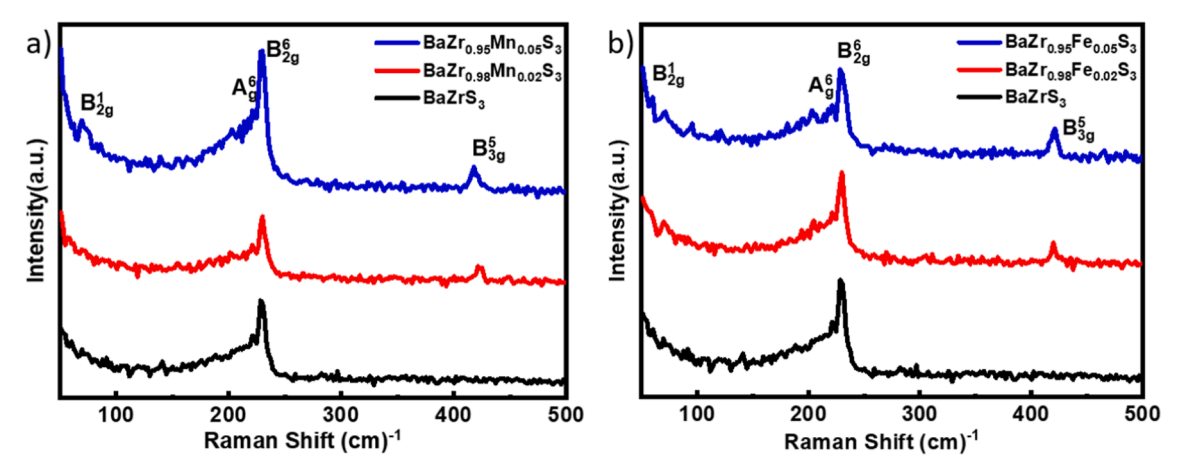


Fig. 2. Raman spectra of a) $Ba(Zr_{1-x}Mn_x)S_3$ and b) $Ba(Zr_{1-x}Fe_x)S_3$ for $x=0,\,0.02,$ and 0.05, measured at room temperature.

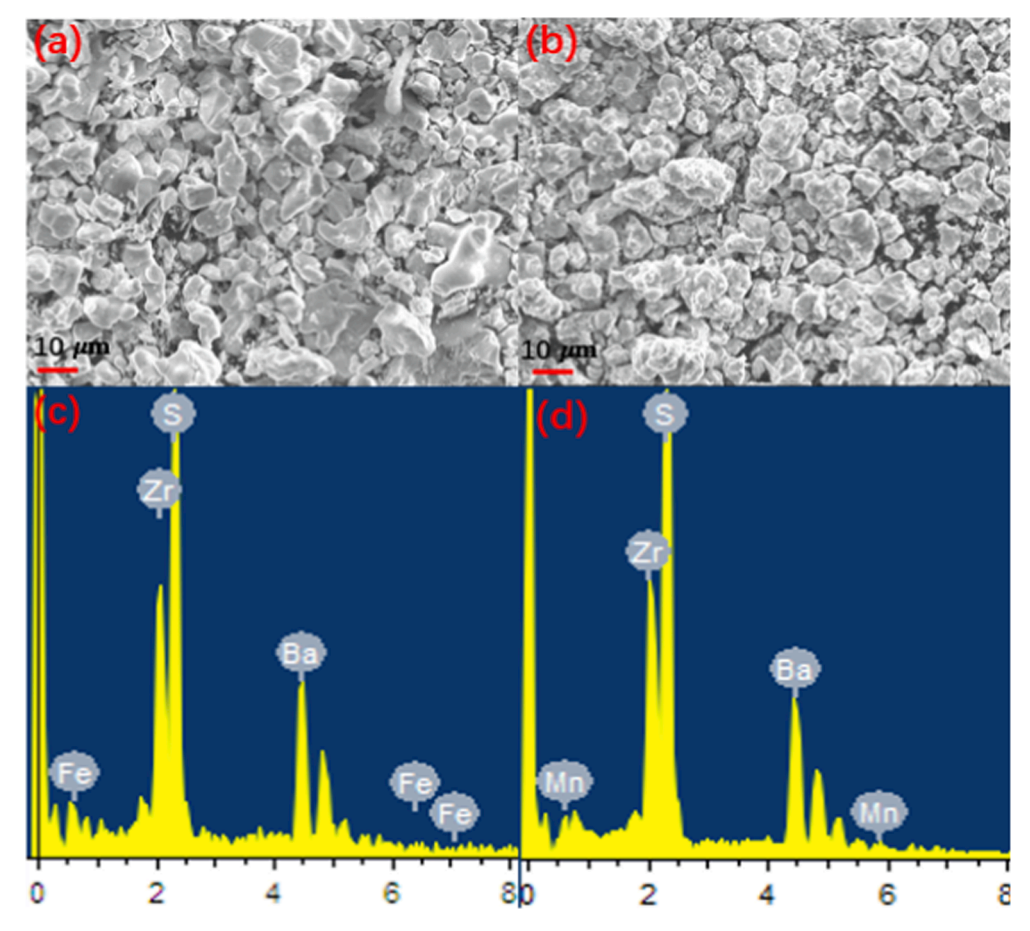


Fig. 3. Typical SEM images of doped powder samples for a) $Ba(Zr_{0.95}Fe_{0.05})S_3$, b) $Ba(Zr_{0.95}Mn_{0.05})S_3$ and the EDX spectra of c) $Ba(Zr_{0.95}Fe_{0.05})S_3$, d) $Ba(Zr_{0.95}Mn_{0.05})S_3$.

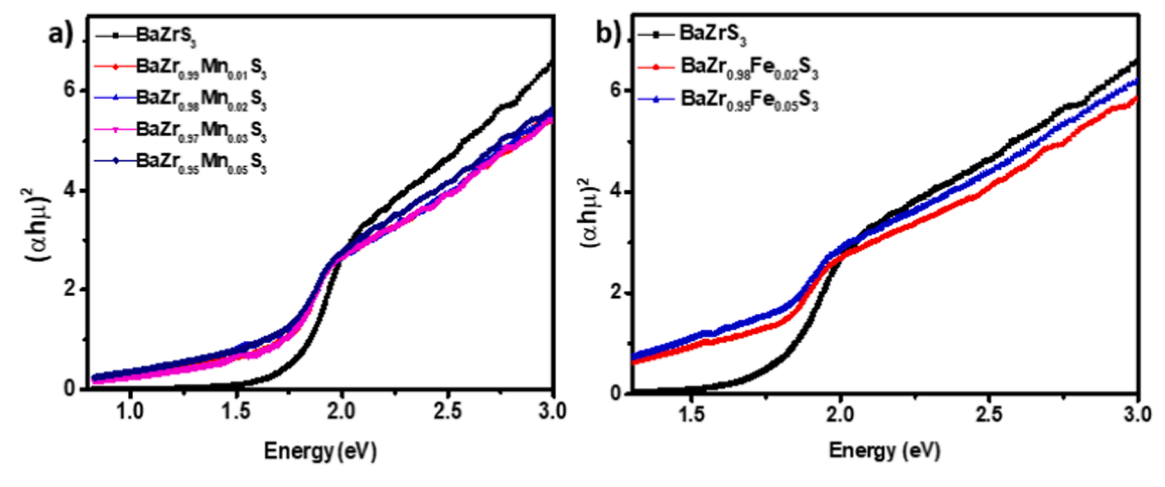


Fig. 4. a) Tauc plot of $Ba(Zr_{1.x}Fe_x)S_3$ powder samples for x=0,0.01,0.02,0.03, and 0.05; b) Tauc plot of $Ba(Zr_{1.x}Fe_x)S_3$ powder samples for x=0,0.02, and 0.05. The tables in the inset show the band gap values extracted from the Tauc plot at different Mn and Fe doping percentage.

300 K, which then increases slightly to 3,840 Oe at 2 K, suggesting strong magnetic anisotropy. The origin of the room temperature ferromagnetic behavior for Fe doped $BaZrS_3$ remains to be unveiled. In conventional DMS materials such as transition metal doped III-V and II-VI semiconductors, magnetism is typically attributed to sp-d exchange interactions between the localized dopants and free carriers in the semiconductor host[3,4,34,35]. In chalcogenide perovskites such as $BaZrS_3$, however, the conduction band edge mainly consists of d states of the B cation[19]. Therefore, the magnetic exchange interactions

between dopant spins are mediated by carriers of d-character, unlike the traditional DMS where sp-states mediate the exchange. A stronger conduction band spin splitting is expected due to the symmetry of mediating d-states, that, in turn, implies a larger induced magnetic moment of the carrier spins and stronger exchange coupling constant. Such a d-d exchange between dopants and carriers may induce larger carrier spin polarization and it can be further controlled by concentrations of dopant and sulfur vacancy. The Curie temperature of such systems could be significantly higher than that of the traditional DMS exhibiting sp-

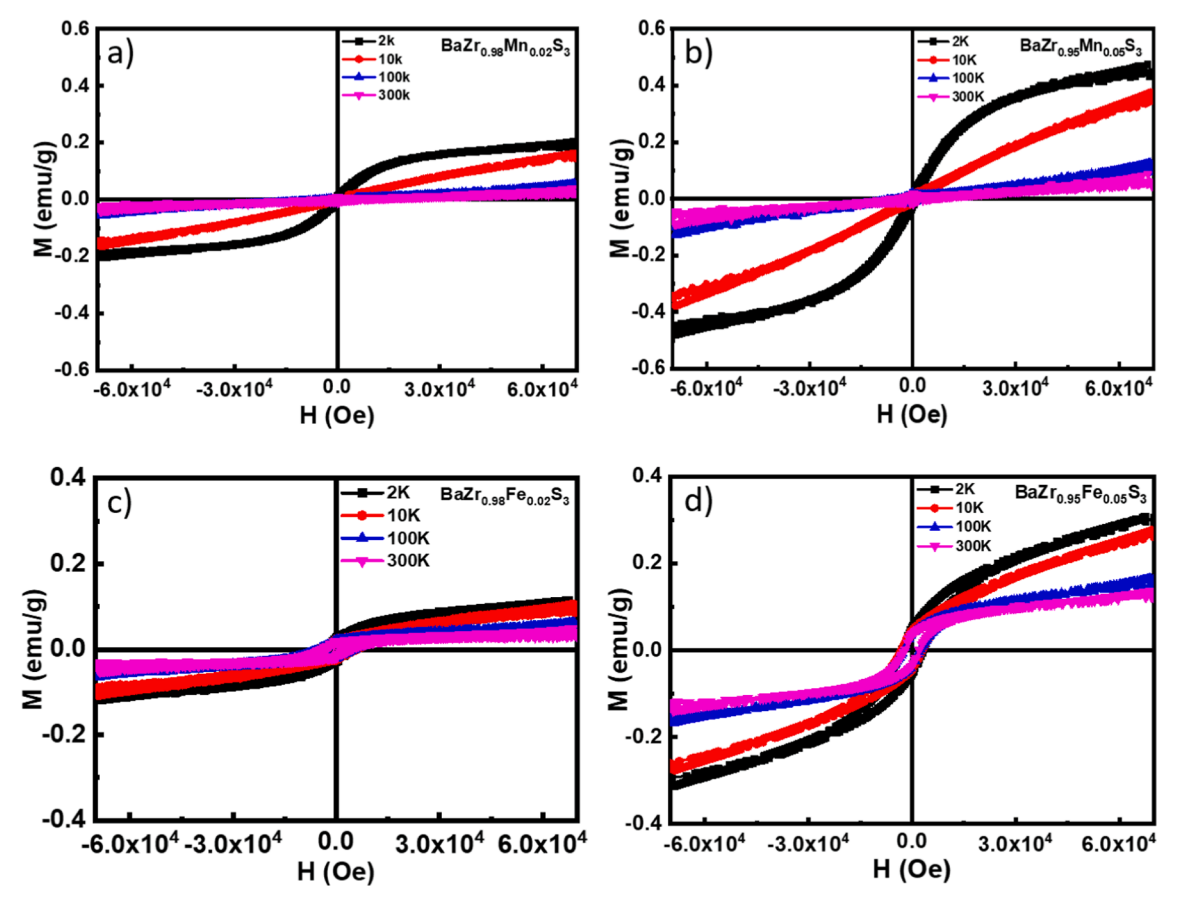


Fig. 5. M-H loop of a) 0.02 and b) 0.05 Mn-doped $Ba(Zr_{1.x}Mn_x)S_3$ as well as c) 0.02 and d) 0.05 Fe-doped $Ba(Zr_{1.x}Fe_x)S_3$ powder samples at 2 K, 10 K, 100 K, and 300 K.

d exchange interactions. We suggest that this might be a viable approach to realize above room temperature magnetic semiconductors. The magnetic interactions may also be attributed to their successive spin polarization as mediated by the sp-orbitals of the first nearest neighbor anions, as theoretically explored in some transition metal oxides [5,6,8]. Further magneto-photoluminescence and transport measurements, together with detailed modeling of magnetic interactions, in BaZrS $_3$ and other related materials, are needed to verify the proposed mechanism, and the presence of carrier spin polarization.

It is important to rule out spurious effects as the origin of the observed ferromagnetism in Ba(Zr_{1-x}Fe_x)S₃. Contaminations, precipitation of secondary phases and defects such as vacancies have all been reported to induce weak ferromagnetism in semiconductors. Since pristine BaZrS₃ shows diamagnetism, and Ba(Zr_{1-x}Mn_x)S₃ and Ba(Zr_{1-x}Fe_x)S₃ exhibit clearly different magnetic behaviors, despite identical processing conditions, this rules out contamination as the source of ferromagnetism in $Ba(Zr_{1-x}Fe_x)S_3$. Moreover, magnetization increases with increasing Fe doping concentration, despite similar sulfur vacancy concentration, which shows that magnetism is associated with Fe dopants instead of sulfur vacancies. Secondary phases such as FeS_x with a variety of stoichiometries such as Fe₇O₈ and Fe₃S₄ are stable and ferrimagnetic with a T_C above room temperature [36,37]. However, these secondary phases were not observed from the XRD spectra up to the detection limit. The substantial sulfur vacancies in the perovskite phase also does not favor the formation of a sulfide impurity phase. Furthermore, there has been no report of a FeS_x phase with strong magnetic anisotropy. Thus, we conclude that the ferromagnetism is intrinsic to Fe-doped chalcogenide perovskite BaZrS₃.

4. Conclusions

In summary, $Ba(Zr_{1-x}Mn_x)S_3$ and $Ba(Zr_{1-x}Fe_x)S_3$ powders with x ranging from 0 to 0.5 were synthesized. XRD and Raman spectroscopies suggest that Mn and Fe can be doped in the perovskite lattice at the B-site, up to a concentration of 5%. The systematic reduction of the bandgap with increasing doping concentration further confirms Zr substitution, which lowers the energy of the conduction band. Fe doped $BaZrS_3$ exhibits room temperature ferromagnetism. This opens up an approach for realizing DMS using chalcogenide perovskite as a new semiconductor host.

CRediT authorship contribution statement

Zhonghai Yu: Investigation, Validation, Methodology, Formal analysis, Writing – review & editing, Visualization. Chenhua Deng: Investigation, Formal analysis, Writing – review & editing, Visualization. Sen Kong: Investigation, Validation, Formal analysis. Haolei Hui: Investigation. Jiale Guo: Investigation. Qizhong Zhao: Investigation. Fanghua Tian: Investigation. Chao Zhou: Investigation. Yin Zhang: Investigation. Sen Yang: Funding acquisition, Writing – review & editing, Supervision. Hao Zeng: Conceptualization, Validation, Methodology, Formal analysis, Writing – original draft, Writing – review & editing, Supervision, Funding acquisition.

Declaration of Competing Interest

The authors declare that they have no known competing financial interests or personal relationships that could have appeared to influence the work reported in this paper.

Acknowledgments

This work was supported by the National Key R&D Program of China (2021YFB3501401), National Natural Science Foundation of China (Grant No. 52002266, 91963111), Postdoctoral Research Foundation of China (Grant No. 2020M673384), US Ntional Science Foundation ECCS-2042085, CBET-1510121MRI- 1229208, Key Scientific and Technological Innovation Team of Shaanxi province (2020TD-001), Innovation Capability Support Program of Shaanxi (No.2018PT-28, 2017KTPT-04), the Fundamental Research Funds for the Central Universities (China), the World-Class Universities (Disciplines), the Characteristic Development Guidance Funds for the Central Universities.

Appendix A. Supplementary data

Supplementary data to this article can be found online at https://doi.org/10.1016/j.jmmm.2022.169886.

References

- I. Žutić, J. Fabian, S. Das Sarma, Spintronics: Fundamentals and applications, Reviews of Modern Physics, 76(2) (2004) 323-410.
- [2] S. Wolf, et al., Spintronics: a spin-based electronics vision for the future. 294(5546) (2001) 1488-1495.
- [3] T. Dietl, H. Ohno, Dilute ferromagnetic semiconductors: Physics and spintronic structures, Rev. Mod. Phys. 86 (1) (2014) 187–251.
- [4] J.K. Furdyna, Diluted magnetic semiconductors, J. Appl. Phys. 64 (4) (1988) R29–R64.
- [5] A.N. Andriotis, M. Menon, Codoping induced enhanced ferromagnetism in diluted magnetic semiconductors, J. Phys.: Condens. Matter 33 (39) (2021) 393002, https://doi.org/10.1088/1361-648X/ac0851.
- [6] A.N. Andriotis, M. Menon, Successive spin polarization contribution to the magnetic coupling in diluted magnetic semiconductors: A quantitative verification, J. Magn. Magn. Mater. 501 (2020) 166313, https://doi.org/10.1016/j. immm 2019 166313
- [7] X. Meng, Y. Liu, G. Han, W. Yang, Y. Yu, Three-dimensional (Fe3O4/ZnO)@C Double-core@shell porous nanocomposites with enhanced broadband microwave absorption, Carbon 162 (2020) 356–364.
- [8] A.N. Andriotis, M. Menon, Defect-induced magnetism: Codoping and a prescription for enhanced magnetism, Phys. Rev. B 87 (15) (2013), 155309.
- [9] Y. Deng, Y. Yu, Y. Song, J. Zhang, N.Z. Wang, Z. Sun, Y. Yi, Y.Z. Wu, S. Wu, J. Zhu, J. Wang, X.H. Chen, Y. Zhang, Gate-tunable room-temperature ferromagnetism in two-dimensional Fe3GeTe2. Nature 563 (7729) (2018) 94–99.
- $[10]\;$ K.J.S. Ando, Seeking room-temperature ferromagnetic semiconductors. 312(5782) (2006) 1883-1885.
- [11] Y. Matsumoto, M. Murakami, T. Shono, T. Hasegawa, T. Fukumura, M. Kawasaki, P. Ahmet, T. Chikyow, S.-y. Koshihara, H. Koinuma, Room-temperature ferromagnetism in transparent transition metal-doped titanium dioxide, Science 291 (5505) (2001) 854–856.
- [12] K. Ueda, H. Tabata, T. Kawai, Magnetic and electric properties of transition-metal-doped ZnO films, Appl. Phys. Lett. 79 (7) (2001) 988–990.
- [13] L. Sangaletti, et al., Ferromagnetism on a paramagnetic host background: the case of rutile TM: TiO2 single crystals (TM= Cr, Mn, Fe Co, Ni, Cu), J. Phys.: Condens. Matter 18 (32) (2006) 7643.
- [14] M. Venkatesan, C.B. Fitzgerald, J.M.D. Coey, Unexpected magnetism in a dielectric oxide, Nature 430 (7000) (2004).

- [15] L. Chen, et al., Enhancing the Curie temperature of ferromagnetic semiconductor (Ga, Mn) As to 200 K via nanostructure engineering. 11(7) (2011) 2584-2589.
- 16] K. Sato, H. Katayama-Yoshida, First principles materials design for semiconductor spintronics, Semicond. Sci. Technol. 17 (4) (2002) 367–376.
- [17] W. Liu, H. Zhang, J.-a. Shi, Z. Wang, C. Song, X. Wang, S. Lu, X. Zhou, L. Gu, D. V. Louzguine-Luzgin, M. Chen, K. Yao, N.a. Chen, A room-temperature magnetic semiconductor from a ferromagnetic metallic glass, Nat. Commun. 7 (1) (2016), https://doi.org/10.1038/ncomms13497.
- [18] F. Kabir, et al., Room temperature ferromagnetism in dilute magnetic semiconducting ZnO nanoparticles co-doped with Tb and Fe, J. Mater. Sci.: Mater. Electron. 32 (8) (2021) 10734–10749.
- [19] Y.-Y. Sun, M.L. Agiorgousis, P. Zhang, S. Zhang, Chalcogenide Perovskites for Photovoltaics, Nano Lett. 15 (1) (2015) 581–585.
- [20] S. Perera, H. Hui, C. Zhao, H. Xue, F. Sun, C. Deng, N. Gross, C. Milleville, X. Xu, D. F. Watson, B. Weinstein, Y.-Y. Sun, S. Zhang, H. Zeng, Chalcogenide perovskites an emerging class of ionic semiconductors, Nano Energy 22 (2016) 129–135.
- [21] X. Wei, et al., Realization of BaZrS3 chalcogenide perovskite thin films for optoelectronics, Nano Energy 68 (2020), 104317.
- [22] S. Niu, H. Huyan, Y. Liu, M. Yeung, K. Ye, L. Blankemeier, T. Orvis, D. Sarkar, D. J. Singh, R. Kapadia, J. Ravichandran, Bandgap Control via Structural and Chemical Tuning of Transition Metal Perovskite Chalcogenides, Adv. Mater. 29 (9) (2017) 1604733, https://doi.org/10.1002/adma.v29.910.1002/adma.201604733.
- [23] I. Sadeghi, K. Ye, M. Xu, Y. Li, J.M. LeBeau, R. Jaramillo, Making BaZrS3 Chalcogenide Perovskite Thin Films by Molecular Beam Epitaxy, Adv. Funct. Mater. 31 (45) (2021) 2105563, https://doi.org/10.1002/adfm.v31.4510.1002/adfm.202105563.
- [24] K. Hanzawa, S. Iimura, H. Hiramatsu, H. Hosono, Material design of green-light-emitting semiconductors: Perovskite-type sulfide SrHfS3, J. Am. Chem. Soc. 141 (13) (2019) 5343–5349.
- [25] J.A. Márquez et al., BaZrS3 chalcogenide perovskite thin films by H2S sulfurization of oxide precursors, 12(8) (2021) 2148-2153.
- [26] N. Gross, et al., Stability and band-gap tuning of the chalcogenide perovskite BaZrS 3 in Raman and optical investigations at high pressures. 8(4) (2017) 044014.
- [27] Z. Yu, et al., Chalcogenide perovskite BaZrS3 thin-film electronic and optoelectronic devices by low temperature processing. 85 (2021) 105959.
- [28] M. Surendran, H. Chen, B. Zhao, A.S. Thind, S. Singh, T. Orvis, H. Zhao, J.-K. Han, H. Htoon, M. Kawasaki, R. Mishra, J. Ravichandran, Epitaxial Thin Films of a Chalcogenide Perovskite, Chem. Mater. 33 (18) (2021) 7457–7464.
- [29] X. Wei, et al., Ti-alloying of BaZrS3 chalcogenide perovskite for photovoltaics. 5 (30) (2020) 18579-18583.
- [30] W. Meng, et al., Alloying and defect control within chalcogenide perovskites for optimized photovoltaic application. 28(3) (2016) 821-829.
- [31] G. Long, et al., Carrier-dopant exchange interactions in Mn-doped PbS colloidal quantum dots. 101(6) (2012) 062410.
- [32] K.M. Hanif, R.W. Meulenberg, G.F. Strouse, Magnetic ordering in doped Cd1-x Co x Se diluted magnetic quantum dots, J. Am. Chem. Soc. 124 (38) (2002) 11495–11502.
- [33] J.M.D. Coey, d0 ferromagnetism, Solid State Sci. 7 (6) (2005) 660–667.
- [34] M. Berciu, R. Chakarvorty, Y.Y. Zhou, M.T. Alam, K. Traudt, R. Jakiela, A. Barcz, T. Wojtowicz, X. Liu, J.K. Furdyna, M. Dobrowolska, Origin of magnetic circular dichroism in GaMnAs: giant zeeman splitting versus spin dependent density of states, Phys. Rev. Lett. 102 (24) (2009), https://doi.org/10.1103/PhysRevLett.102.247202.
- [35] F. Muckel, S. Delikanli, P.L. Hernández-Martínez, T. Priesner, S. Lorenz, J. Ackermann, M. Sharma, H.V. Demir, G. Bacher, sp-d Exchange Interactions in Wave Function Engineered Colloidal CdSe/Mn:CdS Hetero-Nanoplatelets, Nano Lett 18 (3) (2018) 2047–2053.
- [36] A.P. Roberts, L. Chang, C.J. Rowan, C.-S. Horng, F. Florindo, Magnetic properties of sedimentary greigite (Fe3S4): An update, Rev. Geophys. 49 (1) (2011), https://doi.org/10.1029/2010RG000336.
- [37] A.V. Powell, et al., Structure and magnetism in synthetic pyrrhotite Fe 7 S 8: A powder neutron-diffraction study, Phys. Rev. B 70 (1) (2004), 014415.